Rapid Synthesis of a Pt_1Ru_1/Carbon Nanocomposite Using Microwave Irradiation: A DMFC Anode Catalyst of High Relative Performance

Deborah L. Boxall,[†] Gregg A. Deluga,[‡] Edward A. Kenik,[§] William D. King,[†] and C. M. Lukehart*,[†]

Department of Chemistry, Vanderbilt University, Nashville, Tennessee 37235, The Corrosion Research Center, Department of Chemical Engineering and Materials Science, University of Minnesota, Minneapolis, Minnesota 55455, and the Metals and Ceramics Division, Oak Ridge National Laboratory, Oak Ridge, Tennessee 37831

Received August 15, 2000

Thermal treatment of (η-C_2H_4)(Cl)Pt(μ-Cl)$_2$Ru(Cl)(η^3:η^3-2,7-dimethyloctadienediyl) (**1**)/Vulcan carbon composites under appropriate oxidizing and reducing conditions using microwave dielectric loss heating affords PtRu/Vulcan carbon nanocomposites consisting of PtRu alloy nanoparticles highly dispersed on a powdered carbon support. Two such nanocomposites containing 16 or 50 wt % total metal and alloy nanoclusters of 3.4- or 5.4-nm average diameter are formed within only 100 or 300 s of total microwave heating. XRD and on-particle EDS analyses reveal that complex **1** serves as a reliable single-source molecular precursor for the formation of PtRu nanoparticles having a nearly 1:1 metal alloy stoichiometry. Preliminary measurements of the catalytic activity of these nanocomposites as supported direct methanol fuel cell (DMFC) anode catalysts indicate that the 50 wt % nanocomposite has a performance superior to that of a 60 wt % commercial catalyst and a normalized performance equivalent to that of a proprietary unsupported Pt_1Ru_1 catalyst.

Introduction

Metal alloy/carbon nanocomposites consisting of metal nanocrystals supported on a carbon powder of high surface area are commonly employed heterogeneous catalysts in both small- and large-scale chemical processes.[1−4] Although alloy colloids are usually prepared by reduction of appropriate mixtures of metal salts, mixed-metal carbonyl cluster complexes have been used as single-source molecular precursors for the formation of various Fe−Ru and Fe−Mn/carbon catalysts of controlled metal stoichiometry.[5−7]

Pt alloy/carbon nanocomposites are receiving much current attention as anode or cathode catalysts for fuel cells. Pt−Ru/carbon nanocomposites are now recognized as highly active anode catalysts for both direct methanol fuel cells (DMFCs) and CO-tolerant proton-exchange membrane (PEM) fuel cells.[8] While results from combinatorial studies indicate that quarternary alloy compositions, such as $Pt_{44}Ru_{41}Os_{10}Ir_5$, might possess superior activity as DMFC anode catalysts,[9] there remains much interest in improving the activity of the more established Pt−Ru binary catalysts.

Unsupported Pt−Ru colloids or Pt−Ru/carbon nanocomposites are usually synthesized by either reductive co-deposition of Pt and Ru from mixtures of aqueous salt solutions or by co-deposition of Pt and Ru from aqueous solutions of the sulfito complexes, $Na_6[Pt(SO_3)_4]$ and $Na_4[Ru(SO_3)_3]$, following the Watanabe procedure.[10] More recently, Nuzzo and Shapley have reported that the Pt−Ru carbonyl cluster complexes, $PtRu_5C(CO)_{16}$

* To whom correspondence should be addressed.
[†] Vanderbilt University.
[‡] University of Minnesota.
[§] Oak Ridge National Laboratory.

(1) Bird, A. J. In *Catalyst Supports and Supported Catalysts: Theoretical and Applied Concepts*; Stiles, A. B., Ed.; Buttersworth: Boston, 1987; pp 107−137.
(2) Satterfield, C. N. *Heterogeneous Catalysis in Industrial Practice*; McGraw-Hill: New York, 1991.
(3) (a) Sinfelt, J. H. *Bimetallic Catalysts: Discoveries, Concepts, and Applications*; Wiley: New York, 1983. (b) Ponec, V. *Adv. Catal.* **1983**, *32*, 149.
(4) Moser, W. R., Ed. *Advanced Catalysts and Nanostructured Materials*; Academic Press: San Diego, 1996.
(5) Ichikawa, M. *Adv. Catal.* **1992**, *38*, 283.
(6) Kaminsky, M.; Yoon, K. J.; Goeffroy, G. L.; Vannice, M. A. *J. Catal.* **1985**, *91*, 338.
(7) Venter, J.; Kaminsky, M.; Geoffroy, G. L.; Vannice, M. A. *J. Catal.* **1987**, *103*, 450.
(8) (a) Hamnett, A. *Catal. Today* **1997**, *38*, 445. (b) Hogarth, M. P.; Hards, G. A. *Platinum Metals Rev.* **1996**, *40*, 150. (c) Chandler, G. K.; Genders, J. D.; Pletcher, D. *Plat. Met. Rev.* **1997**, *41*, 54. (d) Ralph, T. R. *Plat. Met. Rev.* **1997**, *41*, 102. (e) Hamnett A.; Troughton, G. L. *Chem. Ind.* **1992**, 480. (f) Ren, X.; Wilson, M. S.; Gottesfeld, S. *J. Electrochem. Soc.* **1996**, *143*, L12. (g) Hogarth, M. P.; Christensenand, P. A.; Hammet, A. *Proc. First Intern. Symp. New Mater. Fuel Cells* **1995**, 310. (h) Lin, W. F.; Wang, J. T.; Savinell, R. F. *J. Electrochem. Soc.* **1997**, *144*, 1917. (i) Gasteiger, H. A.; Markovic, N.; Ross, P. N., Jr.; Cairns, E. J. *J. Electrochem. Soc.* **1994**, *141*, 1795. (j) Surampudi, S.; Narayanan, S. R.; Vamos, E.; Frank, H.; Halpert, G.; LaConti, A.; Kosek, J.; Surya Prakash, G. K.; Olah, G. A. *J. Power Sources* **1994**, *47*, 377. (k) Wang, K.; Gasteiger, H. A.; Markovic, N. M.; Ross, P. N., Jr. *Electrochim. Acta* **1996**, *41*, 2587. (l) Pathanjali, G. A.; Krishnamurthy, B.; Chireau, R. F.; Mital, C. K. *Bull. Electrochem.* **1996**, *12*, 193.
(9) (a) Reddington, E.; Sapienza, A.; Gurau, B.; Viswanathan, R.; Sarangapani, S.; Smotkin, E. S.; Mallouk, T. E. *Science* **1998**, *280*, 1735. (b) Gurau, B.; Viswanathan, R.; Liu, R.; Lafrenz, T.; Lye, K. L.; Smotkin, E. S.; Reddington, E.; Sapienza, A.; Chan, B. C.; Mallouk, T. E.; Sarabgapani, S. *J. Phys. Chem. B* **1998**, *102*, 9997.
(10) Watanabe, M.; Uchida, M.; Motoo, S. *J. Electroanal. Chem.* **1987**, *229*, 395.

10.1021/cm000652m CCC: $20.00
Published on Web 01/27/2001

and $Pt_2Ru_4(CO)_{16}$, can serve as single-source molecular precursors for the preparation of $PtRu_5$ and $PtRu_2$/carbon nanocomposites.[11a−c] These alloy compositions are Ru-rich, and the metal loading of the resulting nanocomposites are typically 1−2 wt %. Pt−Ru nanoparticles having a range of alloy stoichiometries have also been prepared by solution decomposition of mixtures of the dual-source molecular precursors, Pt(dibenzylidene acetone)$_2$ and Ru(η^4-1,5-cyclooctadiene-(η^6-1,3,5-cyclooctatriene), in the presence of poly(vinylpyrrolidone).[11d]

We are currently developing new synthetic strategies for the preparation of Pt−Ru/carbon nanocomposites that specifically exhibit high performance as DMFC anode catalysts. Although fuel cell catalysts are believed to undergo chemical modification during cell fabrication and aging, a correlation of actual DMFC performance with the composition and nature of the initial nanocomposite precatalyst is highly desired to aid the discovery of improved catalysts. Highly active supported catalysts have the additional practical value of reducing the noble metal requirement of operating fuel cells.

Devising synthetic methods for the preparation of Pt−Ru/carbon nanocomposites in which the Pt−Ru alloy nanoclusters have (1) compositions of at least 50 atomic percent Pt, (2) uniform alloy stoichiometry throughout the bulk sample on the nanoscale, (3) an average particle size near 5 nm,[12] and (4) total metal loadings sufficiently high to give acceptable performance in an operating DMFC remains a challenging goal. We are exploring the use of predominantly *noncluster*, mixed-metal complexes as single-source molecular precursors for the preparation of Pt−Ru/carbon nanocomposites that meet these requirements. Preliminary communications of the results of this ongoing investigation are available.[13]

In this report, we describe the preparation of a Pt_1Ru_1/carbon nanocomposite using (η-C_2H_4)(Cl)Pt(μ-Cl)$_2$Ru(Cl)(η^3:η^3-2,7-dimethyloctadienediyl) as a noncluster, 1:1 Pt:Ru bimetallic molecular precursor. Vulcan carbon (Cabot Corporation, XC72R) serves as the traditional carbon powder support. Microwave dielectric loss heating permits rapid conversion of precursor/carbon composites to the desired nanocomposites under appropriate conditions. On-particle EDS measurements reveal Pt/Ru stoichiometries for individual alloy nanocrystals close in value to the bulk metal stoichiometry of the nanocomposite and to the metal stoichiometry of the molecular precursor. Nanocomposites are prepared with arbitrary total metal loadings of 16 and 50 wt % having metal alloy nanocrystals of 3.4- and 5.4-nm average diameters, respectively. The performance of these nanocomposites as DMFC anode catalysts relative to that of two commercially available Pt_1Ru_1/Vulcan carbon catalysts and a proprietary unsupported Pt_1Ru_1 catalyst is also reported. While the nanocomposite of 16 wt % metal loading shows catalytic performance comparable to that of related commercial catalysts, the nanocomposite of 50 wt % metal loading exhibits a much higher performance than that of a commercial supported catalyst having higher metal loading and a normalized performance equivalent to that of a proprietary unsupported Pt_1Ru_1 catalyst.

Experimental Section

General Methods. ^{1}H NMR spectra were recorded on a Bruker AC300 Fourier transform spectrometer operating at 300 MHz, using the ^{2}H signal of the solvent as the internal lock frequency. Solvents were distilled over appropriate drying agents prior to use.[13e]

Samples for transmission electron microscopy (TEM) imaging were prepared by placing a drop of a nanocomposite/CH_2Cl_2 suspension onto a holey carbon-coated, copper grid followed by evaporation of the solvent. Particle-size distributions for the nanocomposite materials were obtained by manually measuring over 150 particles from bright-field micrographs recorded on a Philips CM20T TEM operating at 200 kV.

Single-particle high-spatial resolution energy-dispersive spectroscopy (HR-EDS) was used to examine individual nanoparticle compositions using a Philips CM200FEG 200kV TEM equipped with an Oxford light-element EDS detector and an EMiSPEC Vision integrated data acquisition system in the Shared Research Equipment Facility of the Metals and Ceramics Division of ORNL. The HR-EDS data were collected using a tilt angle of 35°, an acceleration voltage of 200 kV, and a collection time of 20 s with a 1.4-nm diameter probe in the stopped-scan mode. Integrated intensities for the Pt Lα_1 and the Ru K$\alpha_{1,2}$ emissions were calibrated using standard procedures and a complex **1**/Vulcan carbon composite as a standard.[14]

X-ray diffraction (XRD) scans were obtained using a Scintag X_1 θ/θ automated powder X-ray diffractometer with a Cu target, a Peltier-cooled solid-state detector, and a zero-background, Si(510) sample support. X-ray photoelectron spectroscopic (XPS) analyses were performed on a PHI 5400 XPS instrument using Mg Kα X-rays. Samples were mounted on copper high-vacuum tape (3M Corporation). XPS data were acquired from a 3 × 10 mm sample area. Samples were introduced into the main chamber at pressures less than 1×10^{-8} Torr. The base pressure in the chamber was 1.2×10^{-10} Torr. The operating pressure was 1×10^{-9} Torr.

Thermogravimetric analyses (TGA) were performed on a TA Instruments high-resolution TGA Model 2950. Bulk elemental analyses were performed by Galbraith Laboratories, Knoxville, TN, and by VHG Labs, Inc., Manchester, NH.

Preparation of (η-C_2H_4)(Cl)Pt(μ-Cl)$_2$Ru(Cl)(η^3:η^3-2,7-Dimethyloctadienediyl), 1. Precursor **1** was prepared from [(η-C_2H_4)ClPt(μ-Cl)]$_2$ (Strem Chemical Co.) and [(η^3:η^3-2,7-dimethyloctadienediyl)ClRu(μ-Cl)]$_2$,[15] using a modification of the procedure reported by Severin for the preparation of analogous Pt−Ru bimetallic complexes.[16] Specifically, 0.640 g (1.06 mmol) of [(η-C_2H_4)ClPt(μ-Cl)]$_2$ and 0.637 g (1.03 mmol) of [(η^3:η^3-2,7-dimethyloctadienediyl)ClRu(μ-Cl)]$_2$ were placed in a round-bottom flask and were dissolved in ≈75 mL of CH_2Cl_2. The solution was left stirring for several hours under a

(11) (a) Nashner, M. S.; Frenkel, A. I.; Adler, D. L.; Shapley, J. R.; Nuzzo, R. G. *J. Am. Chem. Soc.* **1997**, *119*, 7760. (b) Nashner, M. S.; Frenkel, A. I.; Somerville, D.; Hills, C. W.; Shapley, J. R.; Nuzzo, R. G. *J. Am. Chem. Soc.* **1998**, *120*, 8093. (c) Hills, C. W.; Nashner, M. S.; Frenkel, A. I.; Shapley, J. R.; Nuzzo, R. G. *Langmuir* **1999**, *15*, 690. (d) Pan, C.; Dassenoy, F.; Casanove, M. J.; Philippot, K.; Amiens, C.; Lecante, P.; Mosset, A.; Chaudret, B. *J. Phys. Chem. B* **1999**, *103*, 10098.

(12) Mukerjee, S.; McBreen, J. *J. Electroanal. Chem.* **1998**, *448*, 163.

(13) (a) King, W. D.; Lukehart, C. M. *Abstr. Pap. Am. Chem. Soc.* **1998**, *215* (Pt. 1), 114-INOR. (b) Boxall, D. L.; Corn, J. D.; Lukehart, C. M. *Abstr. Pap. Am. Chem. Soc.* **1998**, *215* (Pt. 1), 346-INOR. (c) Boxall, D. L.; King, W. D.; Lukehart, C. M. *Abstr. Pap. Am. Chem. Soc.* **1998**, *216*, 67-MTLS. (d) Boxall, D. L.; Corn, J. D.; Jones, E. F., III.; King, W. D.; Lukehart, C. M. *1998 Fuel Cell Seminar Abst.* **1998**, 545. (e) Lukehart, C. M.; Boxall, D. L.; Corn, J. D.; Hariharasarma, M.; King, W. D.; Kwiatkowski, K. C.; Steigerwalt, E. S.; Kenik, E. A. *Am. Chem. Soc. Fuel Chem. Div. Prepr.* **1999**, *44* (4), 982.

(14) Williams, D. B.; Carter, C. B. *Transmission Electron Microscopy*; Plenum: New York, 1996; pp 605−607.

(15) Cox, D. N.; Roulet, R. *Inorg. Chem.* **1990**, *29*, 1360.

(16) Severin, K.; Polborn, K.; Beck, W. *Inorg. Chim. Acta* **1995**, *240*, 339.

nitrogen atmosphere. The solvent was removed at reduced pressure from the reddish-brown solution to give a brown powder. Recrystallization from methylene chloride/hexane solution gave 1.187 g (1.97 mmol, 95% yield) of **1** as red-purple microcrystals (mp 140−146 °C). Spectroscopic data indicated that a small amount of a second isomer was also present in the sample. The isomer in which the C_2H_4 and $C_{10}H_{16}$ ligands occupy mutually trans orientations is most often observed for this type of complex but isomeric mixtures have been reported as well.[16] Spectroscopic data for the major isomer of complex **1** are the following: ^{1}H NMR [300 MHz, $CDCl_3$]: δ 2.34 (*s*, $CH_2CHC(CH_3)CH_2$, 3H), 2.36 (s, $CH_2CHC(CH_3)CH_2$, 3H), 2.44 (m, $CH_2CHC(CH_3)CH_2$, 2H), 2.6−2.9 (m, $CH_2CHC(CH_3)CH_2$, 2H), 4.55 (m, $CH_2CHC(CH_3)CH_2$, 1H), 4.68 (s, C_2H_4, 4 H), 5.00 (s, $CH_2CHC(CH_3)CH_2$, 1H), 5.06 (m, $CH_2CHC(CH_3)CH_2$, 1H), 5.31 (s, $CH_2CHC(CH_3)CH_2$, 1H), 5.60 (s, $CH_2CHC(CH_3)CH_2$, 1H), 6.03 (s, $CH_2CHC(CH_3)CH_2$, 1H). ^{13}C NMR [75 MHz, $CDCl_3$]: δ 19.8 and 20.5 ($CH_2CHC(CH_3)CH_2$), 34.1 and 35.1 ($CH_2CHC(CH_3)CH_2$), 83.3 and 86.5 ($CH_2CHC(CH_3)CH_2$), 93.5 and 95.1 ($CH_2CHC(CH_3)CH_2$), 125.5 and 127.8 ($CH_2CHC(CH_3)CH_2$). Anal. Calcd for $C_{12}H_{20}Cl_4PtRu$: C, 23.93; H, 3.35. Found: C, 24.43; H, 3.72.

Preparation of the PtRu/Vulcan Carbon Nanocomposites (1a) and (1b). Pt_1Ru_1/Vulcan carbon powder nanocomposites were prepared by thermal treatment of precursor **1**/Vulcan carbon powder composites of arbitrary loading. A specific reaction assembly was used for these preparations. This assembly consisted of a one-half dram glass vial containing a sample of the precursor **1**/Vulcan carbon composite nested within a two-dram glass vial containing additional Vulcan carbon powder that served as a thermal bath. For mechanical stability, the nested vials were placed into a 100-mL glass beaker. Thermal treatment was accomplished by dielectric loss heating of the Vulcan carbon powder support using microwave irradiation (Sharp Corporation, Model R-2M52B) at 2.45 GHz at a fixed power level of 600 W. Control studies using untreated Vulcan carbon indicated that the temperature of the carbon powder in the innermost vial increased rapidly upon microwave irradiation. Prolonged microwave irradiation readily leads to softening of the glass vials, and caution is therefore recommended. Reaction vessels heated by microwave should be allowed to cool before handling. A beaker of cold water is also placed within the microwave oven to protect the oven from irradiation damage. The microwave heating protocol used for nanocomposite syntheses was 30-s irradiation on, 45-s irradiation off, and 20-s irradiation on, giving a final reaction temperature of ≈545 °C.

Thermal treatment of precursor **1**/Vulcan carbon composites by microwave irradiation was conducted under air to oxidatively degrade precursor **1** followed by irradiation under getter gas (10% H_2:90% N_2) to ensure the reduction of any metal ions to metal. Between sequential oxidative thermal treatments, the air atmosphere above the inner sample was replenished by mild flushing. The reaction assembly was evacuated to ≈0.01 mmHg and was back-filled with nitrogen gas between oxidative and reductive thermal treatments to preclude formation of potentially explosive air/hydrogen mixtures. Getter gas was supplied using a partially filled helium-grade balloon at a pressure slightly above 1 atm. The filled balloon was affixed to the mouth of the two-dram outer vial using tape.

A Pt_1Ru_1/carbon powder nanocomposite of 16 wt % total metal (**1a**) was prepared in the following manner. A suspension of 240 mg of Vulcan carbon and 120 mg (0.20 mmol) of **1** dissolved in 30 mL of freshly distilled acetone was stirred for 2 h, and then the excess solvent was removed at reduced pressure. Portions (70 mg) of this precursor **1**/Vulcan carbon composite were placed into the inner vial, filling the vial to a depth of ≈1 cm. This assembly was then nested in a 1-cm deep layer of Vulcan carbon (≈0.15 g) within the outer glass vial.

This reaction assembly was placed into a microwave oven and was irradiated under air for a total of 50 s (30-s irradiation on; 45-s irradiation off; 20-s irradiation on) to effect oxidative degradation of the precursor. The reaction assembly was then irradiated for a total of 50 s under getter gas using the same irradiation protocol. This procedure was repeated until 1.2 g of nanocomposite was obtained. Elemental analysis (wt %) of nanocomposite **1a**: 78.63% C, <0.5% H, 10.77% Pt, and 5.19% Ru.

Table 1. Anode Catalyst Loading for Each Pt−Ru Catalyst Tested

catalyst sample	anode total loading (mg/cm^2)	weight percent metal	anode metal loading (mg/cm^2)
1a	8.3	16	1.33
1b	4.86	50	2.43
E-TEK 30 wt %	8.3	26[a]	2.16
E-TEK 60 wt %	4.52	51[a]	2.31
unsupported PtRu	8.3	100	8.3

[a] As determined from independent elemental analysis (Galbraith Laboratories).

A Pt_1Ru_1/carbon powder nanocomposite of 50 wt % total metal (**1b**) was prepared similarly, utilizing a four-step, sequential deposition of 0.60 g (0.15 g/deposition step) of precursor **1** as an acetone solution onto 0.30 g of the Vulcan carbon support. Between each deposition, the treated carbon was placed into a two-dram vial, which was then nested in a 100-mL beaker containing a 1-cm deep layer (0.7 g) of Vulcan carbon. The entire reaction assembly was then irradiated under air for a total of 50 s (30-s irradiation on; 45-s irradiation off; 20-s irradiation on) to effect oxidative degradation of the precursor. Following the final oxidative step, the two-dram vial was evacuated to ≈0.01 mmHg before back-filling with nitrogen gas. A helium-grade balloon containing getter gas at a pressure slightly above atmospheric was then affixed to the mouth of the vial using tape. The assembly was placed back in the carbon bath and irradiated for an additional 50 s (30-s irradiation on; 45-s irradiation off; 20-s irradiation on) to reduce any metal oxides to metal. A final annealing of the metal nanocomposite was accomplished by back-filling the two-dram vial with nitrogen gas and then affixing a helium-grade balloon containing nitrogen gas to the mouth of the vial. The vial was placed in the carbon bath and was irradiated for an additional 50 s (30-s irradiation on; 45-s irradiation off; 20-s irradiation on). The entire procedure was repeated to give a combined mass of the two nanocomposites of 0.75 g. Elemental analysis (wt %) of nanocomposite **1b**: 41.59% C, <0.5% H, 32.99% Pt, and 16.45% Ru.

For comparative purposes, several other analyses were performed. TGA analysis (TA Instruments, 2950 Hi-Res TGA Analyzer) of untreated commercial Vulcan carbon revealed no significant mass loss up to 500 °C. Elemental analysis of Vulcan carbon: 97.57% C; <0.5% H. Various minerals comprise the remaining mass. Duplicate metal elemental analyses were determined on commercial Pt_1Ru_1/Vulcan carbon catalysts as obtained from E-TEK, Inc. For a 30 wt % total metal loading: 18.29% Pt, 9.20% Ru and 16.50% Pt, 8.97% Ru. For a 60 wt % total metal loading: 31.45% Pt, 16.78% Ru and 35.30% Pt, 18.0% Ru.

Direct Methanol Fuel Cell Testing Procedures. The Pt_1Ru_1/Vulcan carbon nanocomposites **1a** and **1b** were tested as DMFC anode catalysts using standard procedures developed by the Corrosion Research Center at the University of Minnesota. Pt_1Ru_1/Vulcan carbon catalysts having 30 and 60 wt % total metal obtained commercially from E-TEK, Inc., and an unsupported proprietary Pt_1Ru_1 catalyst standard (U.S. Patent No. 5773162) were also tested using identical procedures of anode fabrication and fuel cell operation.

Membrane electrode assemblies (MEAs) were prepared following the procedure described below as 5 × 5 cm squares of active area using a cleaned Nafion 117 membrane as the electrolyte. Anode catalysts were applied to the MEAs at the loadings listed in Table 1. The cathode catalyst was 5.4 mg/cm^2 fuel cell grade platinum as obtained from Johnson Matthey (Stock #12755). Testing was conducted at 90° C using 1.0 M methanol as the fuel. Air at 20 psi gauge pressure and a flow rate of 5 L/min was used as the oxidant.

The following procedure was used for MEA fabrication. The catalyst sample was ultrasonically mixed for 20 min in a clean

bottle with 1200 μL of stock Nafion solution (Aldrich Chemical Co., stock # 27,470-4) and 1200 μL of water. Approximately 2400 μL of 21 wt % isopropyl alcohol in water was added as a diluent to form a well-mixed catalyst ink. A clean, wet Nafion 117 membrane was placed in a frame to secure its swelled dimensions and was then dried with air guns. The catalyst inks were then sprayed onto the Nafion membrane with a modified airbrush. The sprayed ink was dried with air guns upon deposition. Carbon paper (Toray 060) was also sprayed with catalyst ink and was dried on a hot plate (low heating level). The carbon paper was pretreated with a Teflon solution (5 wt %) to make it hydrophobic. Once all catalyst had been spray deposited, the membrane was released from the holder, assembled with the carbon paper, and pressed between two titanium plates at 1300 psi and heated to ≈190 °C under pressure. The MEA was then cooled under pressure and removed from the plates.

Fabricated MEAs were stored in deionized water until testing. The MEA was assembled into the test fixture that utilizes a graphite current collector of a serpentine design for fuel and air distribution and copper end plates. This design is similar to commercially available test fixtures (Electrochem, Inc.). The temperatures of the copper plates and of the fuel solution were carefully controlled and monitored during testing.

The fuel cell was placed in a test stand and was allowed to thermally equilibrate to 90 °C. The airflow was set to 5 L/min with a back pressure of 20 psi gauge. The fuel was pumped through the cell at 140 mL/min. The tank was maintained at 90 °C; a water-cooled condenser open to the atmosphere allowed the release of carbon dioxide and retention of methanol. The fuel cell was allowed to run at open circuit for about 30 min.

When all parameters had reached a steady state, a current load was placed on the cell, and a computer recorded the experimental data (cell voltage, current, temperature of fuel and cell, fuel flow rate, air flow rate, and time). The current load was increased every 5 min until the cell no longer maintained a potential above 100 mV. The data collected were reduced to a polarization curve. The cell was then shut down while at 90 °C, was drained of fuel, and was left overnight to cool to room temperature. The entire polarization curve was then repeated with fresh fuel the following day. Once the fuel cell was cooled and all testing was completed, the MEA was removed from the test fixture and was inspected for breaks, holes, deterioration, or odors.

Results and Discussion

The new 1:1 Pt−Ru binuclear complex, **1**, is readily prepared by metal-fragment metathesis from the corresponding diplatinum and diruthenium complexes shown in eq 1 following the procedure reported by

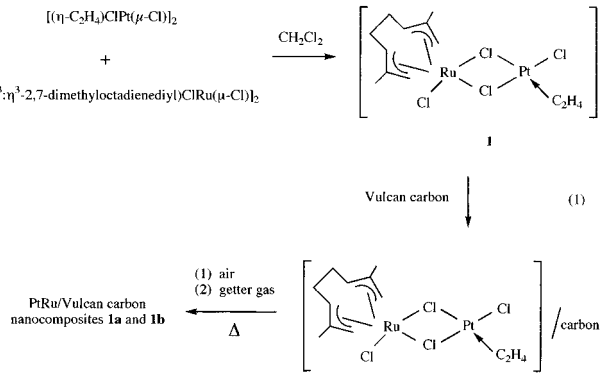

Severin for the preparation of related complexes.[16] Complex **1** is readily soluble in polar organic solvents and can be deposited onto commercial Vulcan carbon powder by adsorption and subsequent solvent evaporation to give precursor **1**/carbon composites of arbitrary, though moderate, loading. Multiple deposition procedures should be followed to obtain highly dispersed metal alloy/carbon nanocomposites at high arbitrary metal loadings (see Experimental Section).

Conversion of precursor **1**/carbon composites to the desired Pt_1Ru_1/Vulcan carbon nanocomposites **1a** and **1b** is accomplished rapidly using dielectric loss heating from microwave irradiation. Vulcan carbon is a highly conductive powder (≈100 S/cm) that is rapidly heated upon exposure to microwave radiation. While microwave heating has been used extensively for chemical synthesis, we believe that this is the first report of using this heating method for the preparation of Vulcan carbon-supported metallic catalysts.[17] Thermal treatment under oxidizing and reducing conditions is employed to ensure chemical degradation of the deposited precursor **1** and formation of alloy nanocrystals.

Nanocomposite **1a** is formed by subjecting a precursor **1**/Vulcan carbon powder composite of appropriate loading to a total of 50 s of microwave irradiation under air and a total of 50 s of microwave irradiation under an atmosphere of getter gas (10% H_2:90% N_2). Bulk elemental analysis of nanocomposite **1a** (Galbraith Laboratories) reveals a total metal content of 16 wt % and a metal stoichiometry of $Pt_{1.08}Ru_1$. Nanocomposite **1b** is prepared similarly using a multideposition protocol to achieve higher metal loading. The overall thermal treatment consists of microwave irradiation periods of 200 s total under air, 50 s under getter gas, and 50 s under a nitrogen atmosphere as a final annealing treatment. Bulk elemental analysis of nanocomposite **1b** (Galbraith Laboratories) reveals a total metal content of 50 wt % and a metal stoichiometry of $Pt_{1.04}Ru_1$.

Duplicate metal analyses of two commercial Pt_1Ru_1/Vulcan carbon catalysts by two independent laboratories (see Experimental Section) give a range of 0.08 for the precision of Pt/Ru atomic ratios determined by elemental analysis. These results suggest that the bulk Pt/Ru atomic ratios determined for nanocomposites **1a** and **1b** are within experimental precision of the expected Pt_1Ru_1 stoichiometry.

TGA analysis of the decomposition of precursor **1** in air shows a smooth, continuous mass reduction consistent with complete loss of all of the organic and chloro ligands. Chlorine is also not evident in the XPS spectra of these nanocomposites. The facile elimination of chlorine from precursor **1** under reactive thermal decomposition is a significant advantage of this synthetic method because experience has shown that even small residual levels of chlorine in DMFC anode catalysts degrades fuel cell performance.

The total metal, carbon, and hydrogen contents of bulk nanocomposites **1a** and **1b** total <100%. In addition to cumulative errors of elemental analysis and a mineral content of ≈2.5 wt % in Vulcan carbon, the remaining nanocomposite mass is assumed to be oxygen. Rolison and co-workers have shown that Pt−Ru/Vulcan carbon nanocomposites undergo significant oxidation of

(17) (a) Galema, S. A. *Chem. Soc. Rev.* **1997**, *26*, 233. (b) Sutton, W. H. *Am. Ceram. Soc. Bull.* **1989**, *68*, 376.

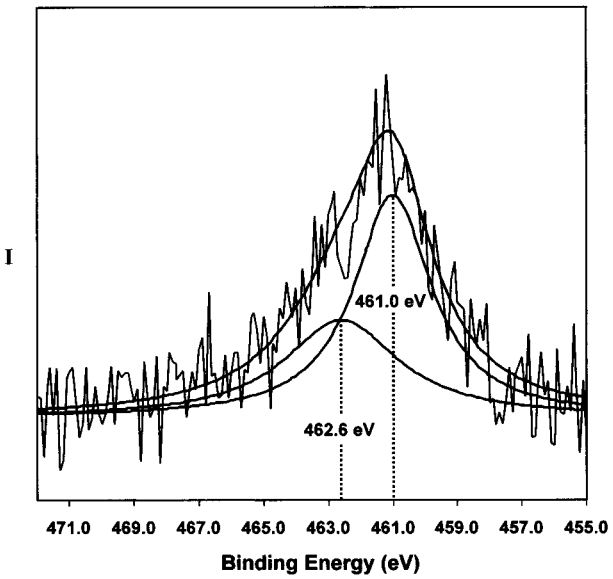

Figure 1. XPS spectrum of the Ru $3p_{3/2}$ photoemission from the Pt_1Ru_1/Vulcan carbon nanocomposite **1b**.

Ru upon exposure to ambient air to form hydrated ruthenium oxide.[18a]

XPS measurements confirm the presence of oxidized Ru in these bulk nanocomposites. The Ru $3p_{3/2}$ photoelectron spectrum of nanocomposite **1b** is shown in Figure 1. Asymmetric broadening of the Ru metal peak at high binding energies is observed, as is characteristic of the presence of oxidized Ru(IV) species. The experimental spectrum can be fit by two overlapping Lorentzian curves centered at 461.0 and 462.6 eV, as shown. Detailed XPS studies of various Ru metal alloy catalysts reveal that Ru $3p_{3/2}$ binding energies of 460.7(3) eV correspond to photoemission from Ru metal and binding energies of 462.7(3) eV correspond to photoemission from oxidized Ru(IV) surface species.[18b,c] For nanocomposite **1b**, the relative intensities of the two observed Ru $3p_{3/2}$ photoemissions gives a Ru(0):Ru(IV) atomic composition of ≈62:38. Unfortunately, the Ru 3d XPS doublet is unresolved and cannot be used for speciation. This observation has been reported by others for similar PtRu/Vulcan carbon nanocomposites.[18d]

Bright-field TEM micrographs of nanocomposites **1a** and **1b** are shown in Figure 2. Metal nanoclusters are imaged in high contrast relative to the amorphous carbon support and are highly dispersed. These metal nanoclusters presumably form through migration and agglomeration of PtRu molecular cores on the carbon surface to give metal alloy nanocrystals. Histograms of metal particle diameters are shown in Figure 3. The observed log-normal particle size distributions are consistent with a coalescence growth mechanism for surface-supported metal particles.[19a] Average metal nanocluster diameters are 3.4 ± 0.9 nm for nanocomposite **1a** and 5.4 ± 3.2 nm for nanocomposite **1b**. The significantly higher total metal loading (50 vs 16 wt %) and prolonged thermal treatment (300 vs 100 s) used in the formation of nanocomposite **1b** probably accounts for the larger nanoclusters observed in this nanocomposite.

A high-resolution TEM micrograph of nanocomposite **1a** is shown in Figure 4. Highly crystalline metal nanocrystals are observed along with particles of the carbon support. Lattice fringes are observed for both the local structure of the graphitic carbon support and the metal nanoparticles. The lattice spacing of 2.23(4) Å observed for the metal particles is consistent with the (111) lattice spacing (2.228 Å) of a face-centered-cubic (fcc) unit cell having a cell constant of 3.862 Å, as expected for a Pt_1Ru_1 alloy.[19b] The metal nanoparticles appear to be nearly entirely crystalline, as evidenced by observing lattice fringes across the full extent of the high-contrast region of particle images. An amorphous surface layer on the metal nanoclusters is not evident by HR-TEM.

An EDS spectrum of nanocomposite **1a** is shown in Figure 5. X-ray emission from a wide area of the sample reveals the emission lines expected for Pt and Ru. Emission from copper is also observed and results from the use of a copper grid to support the nanocomposite in the sample holder.

XRD scans of nanocomposites **1a** and **1b**, shown in Figure 6, reveal diffraction patterns consistent with fcc cells having nearly identical lattice constants of 3.870(9) and 3.862(5) Å, respectively, consistent with crystalline Pt−Ru alloy compositions of $Pt_{0.62}Ru_{0.38}$−$Pt_{0.48}Ru_{0.52}$ for nanocomposite **1a** and $Pt_{0.53}Ru_{0.47}$−$Pt_{0.45}Ru_{0.55}$ for nanocomposite **1b** at the $\pm 1\sigma$ limit.[19b] The broader diffraction peaks for nanocomposite **1a** reflect the smaller average size of the metal alloy nanocrystals in this nanocomposite. A determination of volume-weighted average alloy nanocluster size from XRD peak widths through application of Scherrer's equation gives average nanocluster diameters of 2.9 ± 1.0 nm for nanocomposite **1a** and 8.6 ± 1.9 nm for nanocomposite **1b**.[20] The slightly larger nanocluster size for nanocomposite **1b** as determined by XRD (relative to direct diameter measurements by TEM) probably indicates that metal nanoclusters having diameters significantly greater than the average size are present in the bulk sample. A peak near 43° in 2θ of very weak intensity in the XRD scan of nanocomposite **1b** could indicate the formation of a trace amount of Ru metal and, therefore, some amount of phase separation in this sample.

A determination of the Pt/Ru stoichiometry of individual metal alloy nanoclusters is essential for preparing alloy/carbon nanocomposites of controlled alloy stoichiometry for evaluation as fuel cell catalysts. The integrated intensities of the Pt $L\alpha_1$ and the Ru $K\alpha_{1,2}$ emissions from *individual* alloy nanoclusters in nanocomposites **1a** and **1b** were collected by HR-EDS using a field-emission gun with a spot size of 1.4 nm. Experimental intensities were converted into Pt/Ru atomic ratios using a precursor **1**/Vulcan carbon composite as a standard.

(18) (a) Rolison, D. R.; Hagans, P. L.; Swider, K. E.; Long, J. W. *Langmuir* **1999**, *15*, 774. (b) Huang, C. S.; Houalla, M.; Hercules, D. M.; Kibby, C. L.; Petrakis, L. *J. Phys. Chem.* **1990**, *94*, 6749. (c) Mitchell, P. C. H.; Scott, C. E.; Bonnelle, J. P.; Grimblot, J. G. *J. Catal.* **1987**, *107*, 482. (d) Goodenough, J. B.; Hamnett, A.; Kennedy, B. J.; Manoharan, R.; Weeks, S. A. *J. Electroanal. Chem.* **1988**, *240*, 133.

(19) (a) Granqvist, C. G.; Buhrman, R. A. *J. Catal.* **1976**, *42*, 477. (b) Radmilovic, V.; Gasteiger, H. A.; Ross, P. N., Jr. *J. Catal.* **1995**, *154*, 98.

(20) Prior to peak width measurements diffraction peaks were corrected for background scattering and were stripped of the $K\alpha_2$ portion of the diffraction intensity; see Klug, H. P.; Alexander, L. E. *X-ray Diffraction Procedures for Polycrystalline and Amorphous Materials*, 2nd ed.; Wiley: New York, 1974.

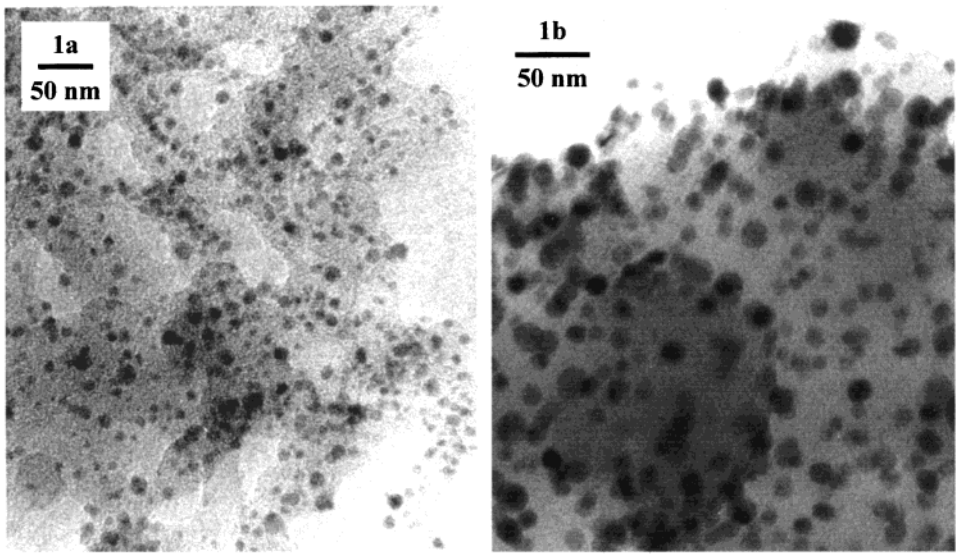

Figure 2. Bright-field TEM micrographs of the Pt_1Ru_1/Vulcan carbon nanocomposites **1a** and **1b**.

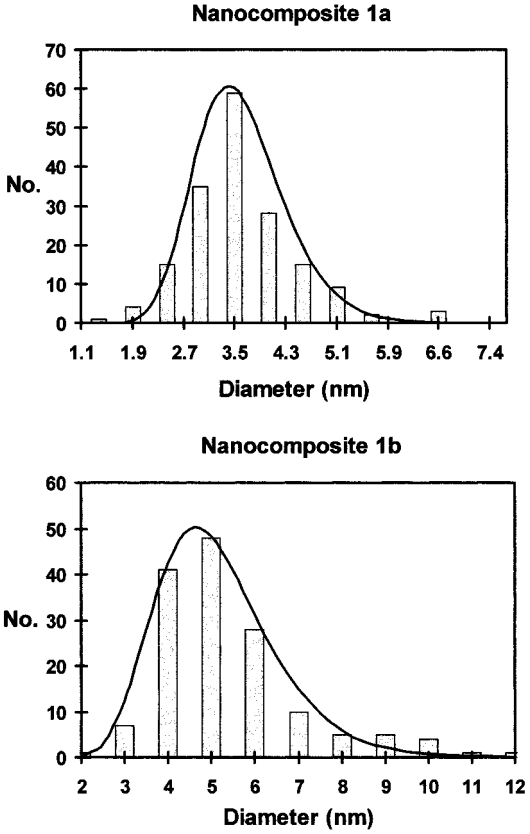

Figure 3. Histograms of metal alloy nanocluster diameters for nanocomposites **1a** (172 particles) and **1b** (157 particles) as measured from TEM micrographs.

Plots of the experimentally determined Pt/Ru atomic ratios of 59 randomly chosen individual nanoclusters of nanocomposite **1a** and for 58 nanoclusters of nanocomposite **1b** are shown in Figure 7 as a function of nanocluster size. Error bars depicted for the Pt/Ru atomic ratios are calculated from error propagation and are based principally on the precision of EDS detection and corrections for X-ray background radiation. Particle-size distributions for those alloy nanoclusters chosen for on-particle HR-EDS measurements are essentially identical to those determined from TEM micrographs (see Figure 3).

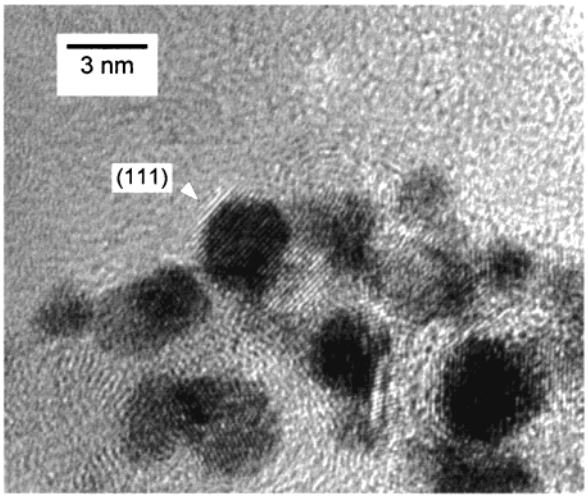

Figure 4. High-resolution TEM micrograph of the Pt_1Ru_1/Vulcan carbon nanocomposite **1a**. Lattice fringes corresponding to the (111) lattice spacings of the alloy nanoparticles are identified by the arrow.

Essentially, all the alloy nanocrystals are enriched in Pt, and many of the smallest alloy particles in both samples show a very high enrichment in Pt. However, no nanoparticles are observed to be Ru-rich. Bulk metal content for nanocomposites **1a** and **1b** calculated using these experimental on-particle metal stoichiometries with appropriate volume-weighting gives alloy stoichiometries of $Pt_{1.64(5)}Ru_1$ and $Pt_{1.57(3)}Ru_1$, respectively. Both of these calculated alloy stoichiometries are inconsistent with the nearly 1:1 Pt/Ru stoichiometry determined experimentally by elemental analysis (Galbraith Laboratories) of these bulk nanocomposites.

It is apparent that some amount of Ru is being lost during HR-EDS analysis due to the rapid and intense local heating caused by the high-flux FEG electron beam (estimated local energy density = 100 MW/mm^2).[21] Repeating the HR-EDS measurements using a sample stage cooled with liquid nitrogen gives little change in the measured on-particle metal stoichiometries, so the

(21) Williams, D. B.; Carter, C. B. *Transmission Electron Microscopy*, Plenum: New York, 1996; 71.

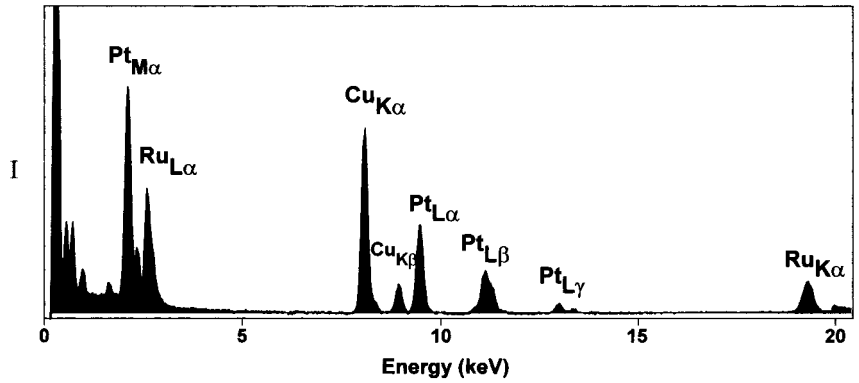

Figure 5. Broad area EDS spectrum of the Pt_1Ru_1/Vulcan carbon nanocomposite **1a**.

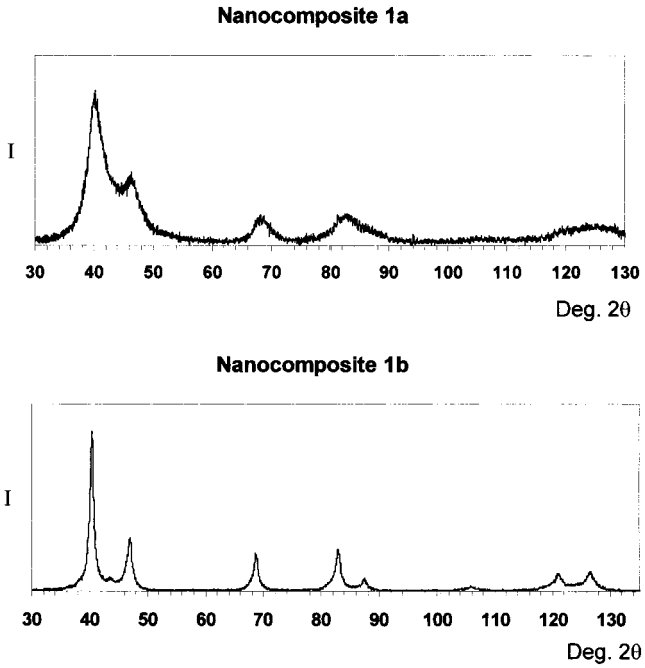

Figure 6. Powder XRD scans for nanocomposites **1a** and **1b**.

local heating effects occurring during beam rastering cannot be suppressed through conductive cooling of the sample. Fortunately, the small spot size of the electron beam does not heat a sufficiently large area during beam rastering to promote nanoparticle sintering.

Experimental on-particle metal stoichiometries have been corrected for Ru loss using a computational model described elsewhere.[22] In this model, each nanocluster is assumed to have a uniform composition of Pt_1Ru_1 and to experience complete Ru loss from an outermost layer of each nanoparticle. The thickness of this outermost layer is calculated via the model such that the mean Pt:Ru ratio of the measured nanoclusters after correction for Ru loss is consistent with the bulk Pt:Ru ratio determined from elemental analysis (Galbraith Laboratories). The calculated amount of Ru lost for each nanocluster is then added to the amount of Ru determined by HR-EDS for that nanoparticle. For nanocomposites **1a** and **1b**, the corresponding Ru-loss layer thicknesses are calculated to be 2.8 and 3.5 Å, respectively.

(22) Boxall, D. L.; Lukehart, C. M.; Kenik, E. A. *Proc. ASME Adv. Energy Syst. Div.* **1999**, *39*, 327.

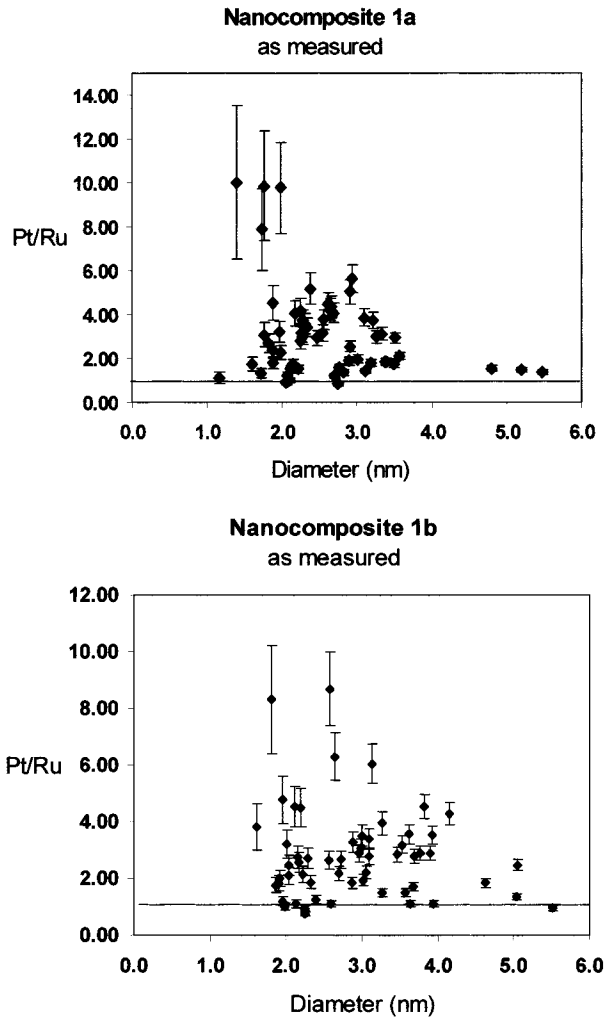

Figure 7. Experimental on-particle Pt/Ru atomic ratios measured by HR-EDS for individual alloy nanoparticles within nanocomposites **1a** and **1b**.

Plots of the corrected Pt/Ru atomic ratios for the individual nanoclusters examined in nanocomposites **1a** and **1b** are shown in Figure 8. These metal stoichiometries are now distributed around the experimentally known bulk metal stoichiometry, and the exceptionally high Pt content observed for the smallest nanoparticles has been adequately compensated. The metal stoichiometry of each nanocomposite sample calculated using these corrected nanoparticle stoichiometries and appropriate volume-weighting is $Pt_{0.8(3)}Ru_1$ for **1a** and $Pt_{0.8(4)}Ru_1$ for **1b**. These calculated bulk stoichiometries

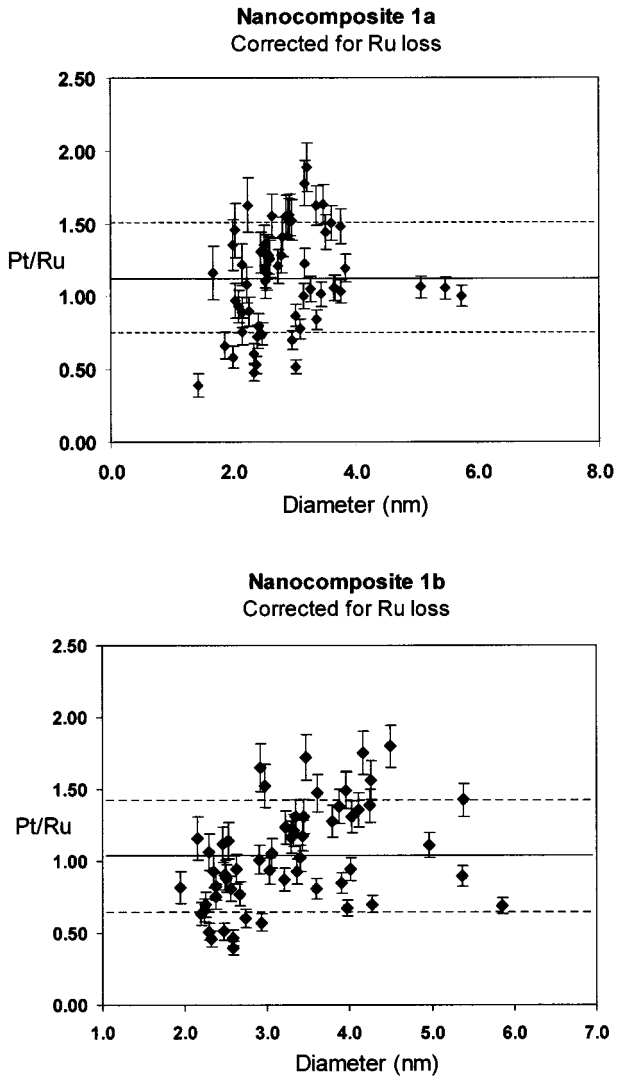

Figure 8. On-particle Pt/Ru atomic ratios measured by HR-EDS and corrected for Ru loss for individual alloy nanoparticles of nanocomposites **1a** and **1b**. Dashed lines indicate the 1σ limit.

are consistent with the values determined experimentally by elemental analysis (Galbraith Laboratories). As a check on the internal consistency of this Ru-loss correction, the calculated loss of 34% of the total Ru present in the measured nanoclusters of nanocomposite **1b** is in excellent agreement with the XPS analysis discussed above in which 38% of the total Ru in nanocomposite **1b** is present as oxidized Ru(IV) species.

As to compositional variation on the nanocluster scale, only statistical arguments can be made. Standard deviations calculated for the mean Pt/Ru atomic ratios of nanocomposites **1a** and **1b** weighted for the experimental uncertainty associated with each on-particle measurement are ± 0.29 and ± 0.36, respectively. These errors are due principally to experimental uncertainties associated with the HR-EDS measurements but also include particle-to-particle variations in alloy stoichiometry. However, this technique does demonstrate that gross phase separation of the two metals between nanoparticles has probably not occurred during the formation of these nanocomposites.

On average, the metal alloy nanoclusters present in nanocomposites **1a** and **1b** appear to have Pt/Ru core compositions not grossly different from 1:1 within the precision of TEM and XRD measurements. These metal cores are highly crystalline as indicated by the high contrast observed for these particles by TEM and by the presence of lattice fringes in HR-TEM images. Because diffracted X-ray intensity is volume-weighted, the observed XRD patterns are consistent with a fcc alloy composition also not grossly different from 1:1. We speculate that the alloy nanoparticles in these samples have an outer layer of approximately one unit cell thickness containing amorphous oxidized Ru and Pt metal that is either highly porous or possibly alloyed to some extent with the particle core. Volume-weighted XRD intensity from such Pt-rich regions would shift the XRD patterns to lower 2θ, giving a slight increase in the calculated fcc lattice constant. Such an effect would be enhanced for nanocomposites having smaller alloy particles on average. Consistent with this prediction, the nanocomposite having a significantly smaller average alloy particle size (**1a**) has the larger calculated lattice constant, although the lattice constants calculated for nanocomposites **1a** and **1b** overlap within a $\pm 1\sigma$ limit. A more precise characterization of alloy nanoparticle composition or surface structure within these samples would require additional investigation.

Nanocomposites **1a** and **1b** have been tested as DMFC anode catalysts and compared to the DMFC performance of two commercial Pt_1Ru_1/Vulcan carbon catalysts (30 and 60 wt % total metal) obtained from E-TEK, Inc.,[23] and one *unsupported* proprietary Pt_1Ru_1 catalyst that is regarded as a catalyst of high performance. All membrane electrode assemblies and test fixtures were fabricated and assembled using a standard procedure. DMFC cell performance was recorded following a standard operating procedure, as described in the Experimental Section. Catalyst identities (and loading in mg of total metal/cm^2 of electrode surface) used in DMFC testing are the following: **1a** (1.33 mg/cm^2); **1b** (2.43 mg/cm^2); 30 wt % E-TEK (2.16 mg/cm^2); 60 wt % E-TEK (2.31 mg/cm^2); and, unsupported catalyst (8.3 mg/cm^2).

Polarization curves for nanocomposite **1b**, the 60 wt % E-TEK supported catalyst, and the unsupported propriety catalyst are shown in Figure 9. Nanocomposite **1b** outperforms the commercial supported catalysts at all recorded current densities. For example, at a cell current density of 300 mA/cm^2, nanocomposite **1b** exceeds the cell potential of the commercial catalyst by 204 mV. Although the unsupported proprietary catalyst outperforms nanocomposite **1b** in this plot, the proprietary catalyst MEA has over 3 times higher anode catalyst loading, as noted in Table 1.

Polarization curves for all five DMFC test cells are shown in Figure 10. For comparison, all current densities have been normalized per milligram of total metal. Nanocomposite **1a** gives an overall cell performance at high current densities essentially equivalent to that of the 60 wt % E-TEK commercial catalyst and a performance between that of the two E-TEK catalysts at lower current densities. However, nanocomposite **1b** gives an

(23) Commercial suppliers of Pt_1Ru_1/VULCAN XC-72R carbon-supported catalysts include: ElectroChem, Inc., Woburn, MA.; E-TEK, Inc., Natick, MA.; Electrosynthesis Co., Inc., Lancaster, NY.; and, Johnson Matthey Plc., Hertfordshire, England.

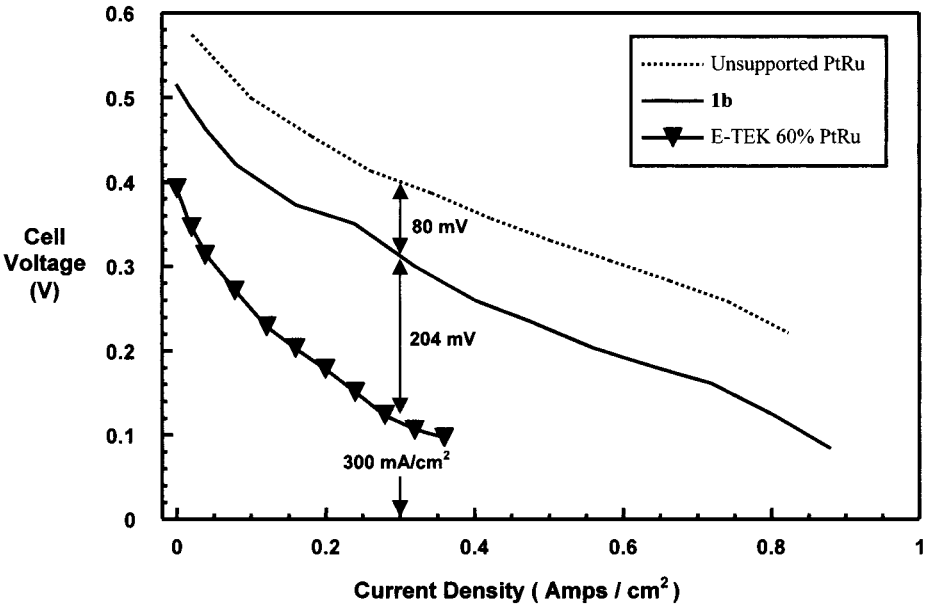

Figure 9. DMFC $i-V$ curves comparing the performance of nanocomposite **1b**, a 60 wt % Pt_1Ru_1/Vulcan carbon commercial catalyst, and a proprietary Pt_1Ru_1 unsupported catalyst as anode catalysts.

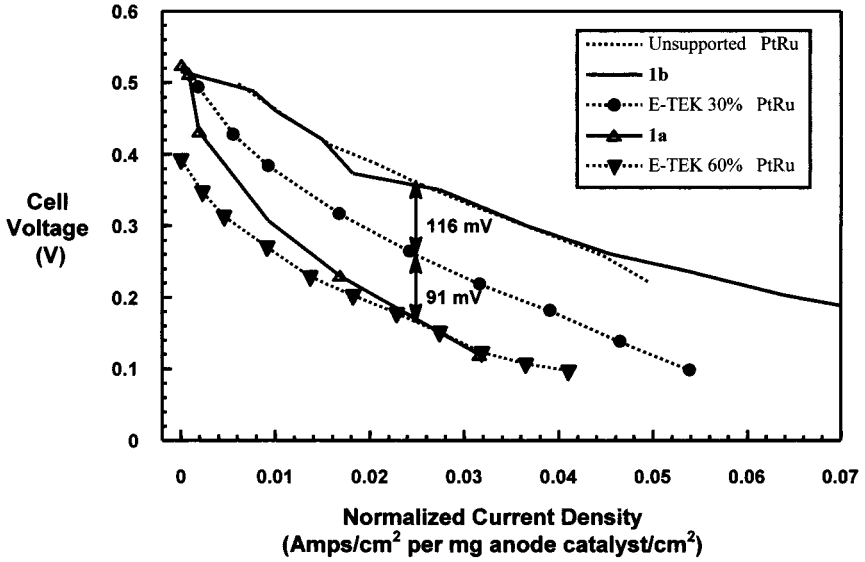

Figure 10. DMFC performance curves normalized per milligram of catalyst comparing the normalized current density of nanocomposites **1a** and **1b** with two commercial E-TEK Pt_1Ru_1/Vulcan carbon catalysts (30 and 60 wt % total metal) and a proprietary unsupported Pt_1Ru_1 catalyst as anode catalysts.

exceptionally high cell performance *essentially equivalent to that of the unsupported catalyst at all current densities*. For example, at 0.35 V this performance is 116 mV higher than that of the 30 wt % E-TEK catalyst and 207 mV higher than that of the other two catalysts tested. Although common experience has often shown that supported catalysts are not as efficient as unsupported catalysts in DMFCs, the $i-V$ curves reported in Figure 8 show that the PtRu particles in the catalyst prepared from nanocomposite **1b** are as effective as those of the best unsupported PtRu catalyst.

An interesting question remains as to why nanocomposite **1b** has a greater normalized performance as a DMFC anode catalyst than does nanocomposite **1a**. We speculate that some feature of the thermal history of nanocomposite **1b** is responsible for its enhanced performance. The multideposition procedure used to prepare nanocomposite **1b** subjects this nanocomposite to three additional air oxidation/getter gas reduction cycles than that experienced by nanocomposite **1a**. Also, nanocomposite **1b** is uniquely subjected to a final thermal annealing under nitrogen. McNicol and Short have reported great enhancement of methanol oxidation activity for PtRu/carbon catalysts following air or nitrogen thermal activation and very low activity following thermal activation under hydrogen.[24] Similar effects would explain the enhanced performance of nanocomposite **1b**.

Studies probing the dependence of DMFC performance on specific preparative conditions used to synthesize Pt−Ru/carbon nanocomposites by this synthetic strategy are underway. However, the successful synthesis of a supported Pt−Ru nanocomposite that exhib-

(24) McNicol, B. D.; Short, R. T. *J. Electroanal. Chem.* **1977**, *81*, 249.

its a DMFC normalized performance equivalent to that of a highly active unsupported Pt−Ru catalyst is very encouraging. Further refinement of preparative procedures including variation of the carbon support material will hopefully afford alloy/carbon nanocomposites that exhibit normalized fuel cell performance greater than that of related unsupported alloy catalysts.

Acknowledgment. Research support provided by the U.S. Army Research Office under Grants DAAH04-95-1-0146, DAAH04-96-1-0179, DAAH04-96-1-0302, and DAAG55-98-1-0362 is gratefully acknowledged by C.M.L. Support from MURI Contract DA/DAAH04-95-1-0094 is gratefully acknowledged by G.A.D. On-particle EDS and HR-TEM measurements performed at the Oak Ridge National Laboratory SHaRE User Facility was sponsored by the Division of Materials Sciences, U.S. Department of Energy, under Contract DE-AC05-96OR22464 with Lockheed Martin Energy Research Corporation and through the SHaRE Program under contract DE-AC05-76OR00033 with Oak Ridge Associated Universities. We thank Dr. T. P. Hanusa for use of a microwave oven, Raul Caretta of the Surface Science Center at the University of Minnesota for assistance in obtaining XPS data, and Dr. D. A. Shores for helpful discussions.

CM000652M